Rail-bridge coupling element of unequal lengths for analysing train-track-bridge interaction systems

Ping Lou[*, 1, 2], Zhi-Wu Yu[1], F. T. K. Au[3]

* Corresponding author, E-mail: pinglou@mail.csu.edu.cn; or pingloucsu@126.com

1. School of Civil Engineering, Railway Campus, Central South University, 22 Shao-shan-nan Road, Changsha, Hunan Province 410075, P. R. China.

2. Key Laboratory of Heavy Railway Engineering Structure of Education Ministry, Railway Campus, Central South University, 22 Shao-shan-nan Road, Changsha, Hunan Province 410075, P. R. China.

3. Department of Civil Engineering, The University of Hong Kong, Pokfulam Road, Hong Kong, P. R. China. E-mail: francis.au@hku.hk

Abstract: This paper presents a rail-bridge coupling element of unequal lengths, in which the length of a bridge element is longer than that of a rail element, to investigate the dynamic problem of train-track-bridge interaction systems. The equation of motion in matrix form is given for a train-track-bridge interaction system with the present element. Numerical examples with two types of bridge models are chosen to illustrate the application of the present element. The numerical results show that, for the same length of rail element, (1) the dynamic responses of train, track and bridge obtained by the present element are almost identical to those obtained by the rail-bridge coupling element of equal length, and (2) compared with the rail-bridge coupling element of equal length, the present element can help to save computer time. Furthermore, the influence of the length of rail element on the dynamic responses of rail is significant. However, the influence of the length of rail element on the dynamic responses of bridge is insignificant. Therefore, the present element with a shorter rail element and a longer bridge element may be adopted to study the dynamic responses of a train-track-bridge interaction system. In addition, the numerical results show that there are deviations of the dynamic responses of vehicle, rail, and bridge based on the one-layer and two-layer track models, and the maximum deviations increase with the increase of the mass of sleeper.

Keywords: finite element method; rail-bridge coupling element; railway bridge; railway track; train

1 Introduction

The dynamic behaviour of railway bridges subjected to a moving loads has long been an interesting topic in the field of civil engineering. Some researchers studied the dynamic problem of railway bridges taking into account the effects of the track structure subjected to a moving vehicle or train. Le et al. [1] reported some numerical work and field measurements on ballast mats on high-speed bridges, where the rail and bridge were modelled as conventional Timoshenko beam elements. Cheng et al. [2] presented a bridge-track-vehicle element with a few single-wheel vehicles for investigating the vibration of railway bridges under a moving train taking into account the response of track structure. Majka et al. [3] proposed a numerical model to simulate the dynamic interaction between a train, rail track and bridge and applied the model to investigate the influence of dynamics effects on the vertical displacements of the Boyne Viaduct, Drogheda, Ireland. Wu and Yang [4] investigated the two-dimensional steady-state response and riding comfort of a train moving over a series of simply supported railway bridges, together with the impact response of the rails and the bridges. Based on the principle of a stationary value of total potential energy of dynamic systems [5, 6], Lou [7] and Lou and Zeng [8] derived the equations of motion in matrix form with time-dependent coefficients for three types of vehicle-track-bridge interaction elements considering one-, two- and four-wheelset vehicle models, in which the dynamic contact forces between the moving vehicle and the rails were considered as internal forces, and studied the dynamic responses of the vehicle-track-bridge interaction system. Furthermore, Lou [9] investigated the dynamic responses of the interaction system consisting of a moving train, track and bridge by using the finite element method. Zhai et al. [10] developed a high-speed train-track-bridge interaction model and analyzed the dynamic train-track-bridge interactive mechanism. Lee et al. [11] proposed a vehicle-track-bridge interaction analysis model and studied the effects of track on the response of bridge by finite element method. Biondi et al. [12] investigated the vibration of railway bridges under moving trains taking into account the track by a component-mode synthesis method. Li et al. [13] established a coupled

dynamic model of a suspension bridge taking into account the track subjected to a moving train and analyzed the dynamic properties of the bridge, track and train when assuming that ICE3 train was moving on the suspension bridge at a speed of 160~300 km/h. Wu et al. [14] developed a vehicle-rail-bridge interaction model for analyzing the three-dimensional dynamic interaction between the moving trains and the railway bridge. Besides the above papers have concerned the dynamic problem of the vehicle-track-bridge interaction, some monographs have devoted this subject. For example, Zhai [15], and Pan and Gao [16] proposed the theory and method for analysing the dynamic problem of the vehicle-track-bridge interaction.

In the aforementioned works, most researchers established the finite element model of the track-bridge interaction system, in which a rail-bridge coupling element of equal length, i.e. with the length of rail element equal to that of bridge element, was adopted. With the length of bridge increases, then the degrees of freedom of the track-bridge interaction system increase. Therefore, the dynamic analysis of a track-bridge interaction system using the rail-bridge coupling element of equal length becomes relatively time consuming. Generally, the flexural rigidity and mass of rail are much smaller than those of bridge. Thus, the aim of this paper is to present a rail-bridge coupling element of unequal length, in which the length of a bridge element is longer than that of a rail element, for investigating the dynamic problem of a track-bridge interaction system subjected to a moving train. The present element not only gives satisfactory results, but also helps to save computer time. In addition, this paper can be regarded as an extension of the theory presented in references [7, 8]. A one-layer track model with sleeper ignored was adopted in references [7, 8], however, a two-layer track model with sleeper considered is applied in this paper. Compared with the former, the latter is close to the practical situation of track and can give the dynamic responses of sleepers. A numerical example is applied to investigate the effects of the two types of track models on the dynamic responses of vehicle, rail, and bridge.

2 A rail-bridge coupling element of unequal lengths

2.1 Model

In the present study, only the dynamic behaviour in the vertical plane is studied, while the axial deformations of rail and bridge are neglected. The two rails of a track are effectively treated as one in the subsequent analysis. Both the rail and bridge deck are modelled as a uniform Bernoulli-Euler beam. Figure 1 shows a typical rail-bridge coupling element of unequal lengths, in which the length of bridge element is longer than that of rail element. The present coupling element consists of several rail elements of equal lengths, a bridge element, a few sleepers, a series of pads modelled as discrete massless springs with stiffness k_{rs} and dampers with damping coefficient c_{rs} connecting rail and sleepers, and a series of ballasts modelled as discrete massless springs with stiffness k_{sb} and dampers with damping coefficient c_{sb} connecting sleepers and bridge deck. In Figure 1, l_{r} denotes the length of rail element (LRE), l_{b} denotes the length of bridge element (LBE), l_{sp} denotes the distance between two adjacent sleepers, and the black dots denote the nodes of the rail and bridge elements. The cubic Hermitian interpolation polynomials are used as shape functions of the rail and bridge elements. As axial deformations are neglected, each node in the rail and bridge elements has two degrees of freedom (DOFs), i.e. a vertical displacement and a rotation about an axis normal to the plane of paper. Each sleeper has only one DOF, i.e. a vertical displacement. Fig. 1 also shows the positive directions of these DOFs, which are measured with reference to their respective vertical static equilibrium positions if applicable. It is assumed that LBE is an integer number of times of LRE.

2.2 Stiffness and damping matrices of discrete massless spring and damper

In the present model, one end point of the discrete massless spring and damper connecting the sleeper has an independent DOF, while the other end point connecting the rail or bridge element has a dependent DOF. Considering the discrete massless spring and damper modelling a pad as shown in Fig. 2 as an example, the lower end point has an independent DOF, i.e. vertical displacement y_{s} of a sleeper, while the upper end point has a dependent DOF, which depends on the four DOFs of the *i*-th rail element. From the energy principle, the

stiffness matrix $\mathbf{k}_{\text{pad}}^{\text{e}}$ of order 5×5 of the discrete spring for a pad can be expressed as

$$\mathbf{k}_{\text{pad}}^{\text{e}}=\begin{bmatrix} k_{\text{rs}}N_{\text{r},1}N_{\text{r},1} & k_{\text{rs}}N_{\text{r},1}N_{\text{r},2} & k_{\text{rs}}N_{\text{r},1}N_{\text{r},3} & k_{\text{rs}}N_{\text{r},1}N_{\text{r},4} & -k_{\text{rs}}N_{\text{r},1} \\ & k_{\text{rs}}N_{\text{r},2}N_{\text{r},2} & k_{\text{rs}}N_{\text{r},2}N_{\text{r},3} & k_{\text{rs}}N_{\text{r},2}N_{\text{r},4} & -k_{\text{rs}}N_{\text{r},2} \\ & & k_{\text{rs}}N_{\text{r},3}N_{\text{r},3} & k_{\text{rs}}N_{\text{r},3}N_{\text{r},4} & -k_{\text{rs}}N_{\text{r},3} \\ & \text{symm.} & & k_{\text{rs}}N_{\text{r},4}N_{\text{r},4} & -k_{\text{rs}}N_{\text{r},4} \\ & & & & k_{\text{rs}} \end{bmatrix}_{\xi=\xi_{\text{rs}}} \tag{1}$$

with

$$N_{\text{r},1}=1-3(\xi/l_{\text{r}})^2+2(\xi/l_{\text{r}})^3 \qquad N_{\text{r},2}=\xi[1-2(\xi/l_{\text{r}})+(\xi/l_{\text{r}})^2]$$

$$N_{\text{r},3}=3(\xi/l_{\text{r}})^2-2(\xi/l_{\text{r}})^3 \qquad N_{\text{r},4}=\xi[(\xi/l_{\text{r}})^2-(\xi/l_{\text{r}})]$$

where ξ_{rs} denotes the distance between the left node of the *i*-th rail element and the discrete spring, as shown in Fig. 2. The damping matrix $\mathbf{c}_{\text{pad}}^{\text{e}}$ of order 5×5 of the discrete damper for a pad can be obtained by simply replacing "k_{rs}" in the corresponding stiffness matrix $\mathbf{k}_{\text{pad}}^{\text{e}}$ of Eq. (1) by "c_{rs}". Similarly, the stiffness matrix $\mathbf{k}_{\text{ballast}}^{\text{e}}$ of order 5×5 of the discrete spring for ballast can be expressed as

$$\mathbf{k}_{\text{ballast}}^{\text{e}}=\begin{bmatrix} k_{\text{sb}} & -k_{\text{sb}}N_{\text{b},1} & -k_{\text{sb}}N_{\text{b},2} & -k_{\text{sb}}N_{\text{b},3} & -k_{\text{sb}}N_{\text{b},4} \\ & k_{\text{sb}}N_{\text{b},1}N_{\text{b},1} & k_{\text{sb}}N_{\text{b},1}N_{\text{b},2} & k_{\text{sb}}N_{\text{b},1}N_{\text{b},3} & k_{\text{sb}}N_{\text{b},1}N_{\text{b},4} \\ & & k_{\text{sb}}N_{\text{b},2}N_{\text{b},2} & k_{\text{sb}}N_{\text{b},2}N_{\text{b},3} & k_{\text{sb}}N_{\text{b},2}N_{\text{b},4} \\ & \text{symm.} & & k_{\text{sb}}N_{\text{b},3}N_{\text{b},3} & k_{\text{sb}}N_{\text{b},3}N_{\text{b},4} \\ & & & & k_{\text{sb}}N_{\text{b},4}N_{\text{b},4} \end{bmatrix}_{\xi=\xi_{\text{bs}}} \tag{2}$$

with

$$N_{\text{b},1}=1-3(\xi/l_{\text{b}})^2+2(\xi/l_{\text{b}})^3 \qquad N_{\text{b},2}=\xi[1-2(\xi/l_{\text{b}})+(\xi/l_{\text{b}})^2]$$

$$N_{\text{b},3}=3(\xi/l_{\text{b}})^2-2(\xi/l_{\text{b}})^3 \qquad N_{\text{b},4}=\xi[(\xi/l_{\text{b}})^2-(\xi/l_{\text{b}})]$$

where ξ_{bs} denotes the distance between the left node of the *i*-th bridge element and the discrete spring, as shown in Fig. 3.

3 Equation of motion for a train-track-bridge interaction system with the present element

By using the energy principle, such as the principle of a stationary value of total potential energy of

dynamic systems [5, 6], one can derive the equation of motion written in sub-matrix form for the train-track-bridge interaction system as shown in Fig. 4 as

$$\begin{bmatrix} \mathbf{M}_{vv} & \mathbf{0} & \mathbf{0} & \mathbf{0} \\ \mathbf{0} & \mathbf{M}_{rr} & \mathbf{0} & \mathbf{0} \\ \mathbf{0} & \mathbf{0} & \mathbf{M}_{ss} & \mathbf{0} \\ \mathbf{0} & \mathbf{0} & \mathbf{0} & \mathbf{M}_{bb} \end{bmatrix} \begin{Bmatrix} \ddot{\mathbf{X}}_v \\ \ddot{\mathbf{X}}_r \\ \ddot{\mathbf{X}}_s \\ \ddot{\mathbf{X}}_b \end{Bmatrix} + \begin{bmatrix} \mathbf{C}_{vv} & \mathbf{C}_{vr} & \mathbf{0} & \mathbf{0} \\ \mathbf{C}_{rv} & \mathbf{C}_{rr} & \mathbf{C}_{rs} & \mathbf{0} \\ \mathbf{0} & \mathbf{C}_{sr} & \mathbf{C}_{ss} & \mathbf{C}_{sb} \\ \mathbf{0} & \mathbf{0} & \mathbf{C}_{bs} & \mathbf{C}_{bb} \end{bmatrix} \begin{Bmatrix} \dot{\mathbf{X}}_v \\ \dot{\mathbf{X}}_r \\ \dot{\mathbf{X}}_s \\ \dot{\mathbf{X}}_b \end{Bmatrix} + \begin{bmatrix} \mathbf{K}_{vv} & \mathbf{K}_{vr} & \mathbf{0} & \mathbf{0} \\ \mathbf{K}_{rv} & \mathbf{K}_{rr} & \mathbf{K}_{rs} & \mathbf{0} \\ \mathbf{0} & \mathbf{K}_{sr} & \mathbf{K}_{ss} & \mathbf{K}_{sb} \\ \mathbf{0} & \mathbf{0} & \mathbf{K}_{bs} & \mathbf{K}_{bb} \end{bmatrix} \begin{Bmatrix} \mathbf{X}_v \\ \mathbf{X}_r \\ \mathbf{X}_s \\ \mathbf{X}_b \end{Bmatrix} = \begin{Bmatrix} \mathbf{F}_v \\ \mathbf{F}_r \\ \mathbf{F}_s \\ \mathbf{F}_b \end{Bmatrix} \tag{3}$$

where **M**, **C** and **K** denote the mass, damping and stiffness sub-matrices respectively, **X** and **F** denote the displacement and force sub-vectors respectively, and the subscripts "v", "r", "s" and "b" denote vehicle, rail, sleeper and bridge, respectively. The formation of Eq. (3) from terms in the previous equations is further explained below.

The stiffness matrix $\mathbf{k}_{pad}^{e}$ in Eq. (1) can be partitioned and used as follows in building up Eq. (3). Elements in the first four rows and the first four columns should be placed in the stiffness sub-matrix $\mathbf{K}_{rr}$. Elements in the first four rows in the last column should be placed in the stiffness sub-matrix $\mathbf{K}_{rs}$. Elements in the first four columns in the last row should be placed in the stiffness sub-matrix $\mathbf{K}_{sr}$. The remaining element k_{rs} should be placed in the stiffness sub-matrix $\mathbf{K}_{ss}$. In a similar manner as $\mathbf{k}_{pad}^{e}$, the damping matrix $\mathbf{c}_{pad}^{e}$ can partitioned into four parts and used as damping sub-matrices $\mathbf{C}_{rr}$, $\mathbf{C}_{rs}$, $\mathbf{C}_{sr}$ and $\mathbf{C}_{ss}$ in Eq. (3).

The stiffness matrix $\mathbf{k}_{ballast}^{e}$ in Eq. (2) can also be partitioned and used in building up Eq. (3). The element k_{sb} in the first row and first column should be placed in the stiffness sub-matrix $\mathbf{K}_{ss}$. Elements in the last four columns of the first row should be placed in the stiffness sub-matrix $\mathbf{K}_{sb}$. Elements in the last four rows of the first column should be placed in the stiffness sub-matrix $\mathbf{K}_{bs}$. Elements in the last four rows

and last four columns should be placed in the stiffness sub-matrix $\mathbf{K}_{\mathrm{bb}}$. In a similar manner as $\mathbf{k}^{\mathrm{e}}_{\mathrm{ballast}}$, the damping matrix $\mathbf{c}^{\mathrm{e}}_{\mathrm{ballast}}$ can partitioned into four parts and used as damping sub-matrices $\mathbf{C}_{\mathrm{ss}}$, $\mathbf{C}_{\mathrm{sb}}$, $\mathbf{C}_{\mathrm{bs}}$ and $\mathbf{C}_{\mathrm{bb}}$ in Eq. (3).

The displacement sub-vectors, the mass, damping and stiffness sub-matrices, and the force sub-vectors of the vehicles, rail, sleepers and bridge are elaborated in the following sections.

3. 1 Displacement vectors

It is assumed the number of vehicles on the track concerned is N_{v}, as shown in Fig. 4. The displacement sub-vector of sleepers $\mathbf{X}_{\mathrm{s}}$ of order $N_{\mathrm{s}} \times 1$ can be written as

$$\mathbf{X}_{\mathrm{s}} = [y_{\mathrm{s}1} \quad y_{\mathrm{s}2} \quad \cdots \quad y_{\mathrm{s}N_{\mathrm{s}}}]^{\mathrm{T}} \tag{4}$$

where N_{s} denotes the total number of sleepers as well as the total number of DOFs of sleepers. To reduce the repetition, the expressions of the displacement sub-vectors $\mathbf{X}_{\mathrm{v}}$ of vehicles, $\mathbf{X}_{\mathrm{r}}$ of rail, and $\mathbf{X}_{\mathrm{b}}$ of bridges are not given here and can be found in reference [9].

3. 2 Sub-matrices of vehicles

The expressions of the mass sub-matrix $\mathbf{M}_{\mathrm{vv}}$, the stiffness sub-matrix $\mathbf{K}_{\mathrm{vv}}$, and the damping sub-matrix $\mathbf{C}_{\mathrm{vv}}$ are also not given here and can be found in reference [9].

3. 3 Sub-matrices of rail

The sub-matrices of rail are marked with subscript "rr". The mass sub-matrix of the rail $\mathbf{M}_{\mathrm{rr}}$ of order $N_{\mathrm{r}} \times N_{\mathrm{r}}$ can be written in terms of the overall mass matrix $\mathbf{M}_{\mathrm{rr1}}$ of the rail itself and the overall mass matrix $\mathbf{M}_{\mathrm{rr2}}$ induced by all wheelset masses as

$$\mathbf{M}_{\mathrm{rr}} = \mathbf{M}_{\mathrm{rr1}} + \mathbf{M}_{\mathrm{rr2}} \tag{5}$$

with $$\mathbf{M}_{\mathrm{rr1}} = \sum_{i=1}^{n_{\mathrm{r}}} \int_0^{l_{\mathrm{r}}} \overline{m}_{\mathrm{r}} \mathbf{N}_{\mathrm{r}i}{}^{\mathrm{T}} \mathbf{N}_{\mathrm{r}i} d\xi$$

$$\mathbf{N}_{\mathrm{r}i} = [0 \quad 0 \quad \cdots \quad 0 \quad N_{\mathrm{r},1} \quad N_{\mathrm{r},2} \quad N_{\mathrm{r},3} \quad N_{\mathrm{r},4} \quad 0 \quad \cdots \quad 0 \quad 0]$$

$$\mathbf{M}_{\mathrm{rr2}} = \sum_{j=1}^{N_\mathrm{v}} \sum_{h=1}^{4} m_\mathrm{w} \cdot \mathbf{N}_{jh}^\mathrm{T} \cdot \mathbf{N}_{jh}$$

$$\mathbf{N}_{jh} = [0 \quad 0 \quad \cdots \quad 0 \quad N_{\mathrm{r},1} \quad N_{\mathrm{r},2} \quad N_{\mathrm{r},3} \quad N_{\mathrm{r},4} \quad 0 \quad \cdots \quad 0 \quad 0]_{\xi=\xi_{jh}} \qquad (h = 1\text{-}4)$$

as elaborated below. The overall mass matrix $\mathbf{M}_{\mathrm{rr1}}$ of the rail itself is obtained by assembling all its element mass matrices $\int_0^{l_\mathrm{r}} \overline{m}_\mathrm{r} \mathbf{N}_{\mathrm{r}i}{}^\mathrm{T} \mathbf{N}_{\mathrm{r}i} d\xi$ of order $N_\mathrm{r} \times N_\mathrm{r}$, in which $\overline{m}_\mathrm{r}$ denotes the rail mass per unit length, and $\mathbf{N}_{\mathrm{r}i}$ (i =1, 2, …, n_r) is the shape function matrix for the *i*-th rail element of order $1 \times N_\mathrm{r}$. It should be noted for $\mathbf{N}_{\mathrm{r}i}$ that, apart from those elements corresponding to four DOFs of the two nodes of the *i*-th rail element, all other elements are zero. In the formulation of the overall mass matrix $\mathbf{M}_{\mathrm{rr2}}$ induced by all wheelset masses, ξ denotes the local coordinate measured from the left node of a beam element; as shown in Fig. 5, the local coordinate ξ_{jh} (h = 1 - 4) denotes the distance between the *h*-th wheelset of the *j*-th vehicle and the left node of the rail element on which the wheelset is acting; and the shape function matrix for the rail element $\mathbf{N}_{jh}$ (h = 1 - 4) of order $1 \times N_\mathrm{r}$ is evaluated at the position of the *h*-th wheelset of the *j*-th vehicle. It should be noted for $\mathbf{N}_{jh}$ (h = 1 - 4) that, apart from those elements corresponding to four DOFs of the two nodes of the rail element on which the *h*-th wheelset of the *j*-th vehicle is acting, all other elements are zero.

The stiffness sub-matrix $\mathbf{K}_{\mathrm{rr}}$ of rail of order $N_\mathrm{r} \times N_\mathrm{r}$ can be similarly expressed in terms of the overall stiffness matrix $\mathbf{K}_{\mathrm{rr1}}$ of the rail itself, the overall stiffness matrix $\mathbf{K}_{\mathrm{rr2}}$ induced by all vehicles and the overall stiffness matrix $\mathbf{K}_{\mathrm{rr3}}$ induced by the stiffness of all pads as

$$\mathbf{K}_{\mathrm{rr}} = \mathbf{K}_{\mathrm{rr1}} + \mathbf{K}_{\mathrm{rr2}} + \mathbf{K}_{\mathrm{rr3}} \tag{6}$$

with $$\mathbf{K}_{\mathrm{rr1}} = \sum_{i=1}^{n_\mathrm{r}} \int_0^{l_\mathrm{r}} E_\mathrm{r} I_\mathrm{r} \mathbf{N}''_{\mathrm{r}i}{}^\mathrm{T} \mathbf{N}''_{\mathrm{r}i} d\xi$$

$$\mathbf{K}_{\mathrm{rr2}} = \sum_{j=1}^{N_\mathrm{v}} \sum_{h=1}^{4} [k_\mathrm{p} \cdot \mathbf{N}_{jh}^\mathrm{T} \cdot \mathbf{N}_{jh} + (c_\mathrm{p} v + m_\mathrm{w} a) \cdot \mathbf{N}_{jh}^\mathrm{T} \cdot \mathbf{N}'_{jh} + m_\mathrm{w} v^2 \cdot \mathbf{N}_{jh}^\mathrm{T} \cdot \mathbf{N}''_{jh}]$$

$$\mathbf{K}_{\mathrm{rr3}} = \sum_{u=1}^{N_\mathrm{s}} k_{\mathrm{rs}} \mathbf{N}_{\mathrm{r},u}^\mathrm{T} \mathbf{N}_{\mathrm{r},u}$$

$$\mathbf{N}_{\mathrm{r},u} = [0 \quad 0 \quad \cdots \quad 0 \quad N_{\mathrm{r},1} \quad N_{\mathrm{r},2} \quad N_{\mathrm{r},3} \quad N_{\mathrm{r},4} \quad 0 \quad \cdots \quad 0 \quad 0]_{\xi=\xi_{\mathrm{r},u}}$$

as elaborated below. The overall stiffness matrix $\mathbf{K}_{\mathrm{rr1}}$ of the rail itself is obtained by assembling all its element stiffness matrices $\int_0^{l_\mathrm{r}} E_\mathrm{r} I_\mathrm{r} \mathbf{N}''^{\mathrm{T}}_{\mathrm{r}i} \mathbf{N}''_{\mathrm{r}i} d\xi$ of order $N_\mathrm{r} \times N_\mathrm{r}$, in which E_r denotes Young's modulus of the rail, I_r denotes the constant moment of inertia of the rail cross section, and the prime denotes differentiation with respect to the local coordinate ξ. In the formulation of the overall stiffness matrix $\mathbf{K}_{\mathrm{rr3}}$ induced by the stiffness of all pads, the shape function matrix $\mathbf{N}_{\mathrm{r},u}$ (u=1, 2, …, N_s) of order $1 \times N_\mathrm{r}$ for the rail element is evaluated at the position of the u-th pad, and $\xi_{\mathrm{r},u}$ denotes the distance between the u-th pad and the left node of the rail element containing the u-th pad, as shown in Fig. 5. It should be noted for $\mathbf{N}_{\mathrm{r},u}$ (u=1, 2, …, N_s) that, apart from those elements corresponding to four DOFs of the two nodes of the rail element containing the u-th pad, all other elements are zero.

Similarly, the damping sub-matrix $\mathbf{C}_{\mathrm{rr}}$ of rail of order $N_\mathrm{r} \times N_\mathrm{r}$ can be written in terms of the overall damping matrix $\mathbf{C}_{\mathrm{rr1}}$ induced by all vehicles and the overall damping matrix $\mathbf{C}_{\mathrm{rr2}}$ induced by the damping of all pads as

$$\mathbf{C}_{\mathrm{rr}} = \mathbf{C}_{\mathrm{rr1}} + \mathbf{C}_{\mathrm{rr2}} \tag{7}$$

with $$\mathbf{C}_{\mathrm{rr1}} = \sum_{j=1}^{N_\mathrm{v}} \sum_{h=1}^{4} (c_\mathrm{p} \cdot \mathbf{N}_{jh}^{\mathrm{T}} \cdot \mathbf{N}_{jh} + 2 m_\mathrm{w} v \cdot \mathbf{N}_{jh}^{\mathrm{T}} \cdot \mathbf{N}'_{jh})$$

$$\mathbf{C}_{\mathrm{rr2}} = \sum_{u=1}^{N_\mathrm{s}} c_\mathrm{rs} \mathbf{N}_{\mathrm{r},u}^{\mathrm{T}} \mathbf{N}_{\mathrm{r},u}$$

3. 4 Sub-matrices of sleepers

The sub-matrices of sleepers are marked with subscript "ss". The mass sub-matrix $\mathbf{M}_{\mathrm{ss}}$, stiffness sub-matrix $\mathbf{K}_{\mathrm{ss}}$, and damping sub-matrix $\mathbf{C}_{\mathrm{ss}}$ of order $N_\mathrm{s} \times N_\mathrm{s}$ of sleepers can be written respectively as

$$\mathbf{M}_{\mathrm{ss}} = \mathrm{diag}[m_s \quad m_s \quad \cdots \quad m_s] \tag{8}$$

$$\mathbf{K}_{\mathrm{ss}} = \mathrm{diag}[k_\mathrm{rs} + k_\mathrm{sb} \quad k_\mathrm{rs} + k_\mathrm{sb} \quad \cdots \quad k_\mathrm{rs} + k_\mathrm{sb}] \tag{9}$$

$$\mathbf{C}_{\mathrm{ss}} = \mathrm{diag}[c_{\mathrm{rs}} + c_{\mathrm{sb}} \quad c_{\mathrm{rs}} + c_{\mathrm{sb}} \quad \cdots \quad c_{\mathrm{rs}} + c_{\mathrm{sb}}] \tag{10}$$

where m_s denotes the mass of each sleeper.

3. 5 Sub-matrices of bridges

The sub-matrices of bridges are marked with subscript "bb". The mass sub-matrix $\mathbf{M}_{\mathrm{bb}}$ of order $\overline{N}_{\mathrm{b}} \times \overline{N}_{\mathrm{b}}$ of bridges can be written as

$$\mathbf{M}_{\mathrm{bb}} = \mathrm{diag}[\mathbf{M}_{\mathrm{b1}} \quad \mathbf{M}_{\mathrm{b2}} \quad \cdots \quad \mathbf{M}_{\mathrm{b}N_{\mathrm{b}}}] \tag{11}$$

where the mass matrix $\mathbf{M}_{\mathrm{b}i}$ (i =1, 2, …, N_{b}) of the *i*-th multi-span continuous bridge of order $\overline{n}_{\mathrm{b}i} \times \overline{n}_{\mathrm{b}i}$ can be written as

$$\mathbf{M}_{\mathrm{b}i} = \sum_{j=1}^{n_{\mathrm{b}i}} \int_0^{l_{\mathrm{b}}} \overline{m}_{\mathrm{b}} \mathbf{N}_{\mathrm{b}j}{}^{\mathrm{T}} \mathbf{N}_{\mathrm{b}j} d\xi \tag{12}$$

with $\mathbf{N}_{\mathrm{b}j} = [0 \quad 0 \quad \cdots \quad 0 \quad N_{\mathrm{b},1} \quad N_{\mathrm{b},2} \quad N_{\mathrm{b},3} \quad N_{\mathrm{b},4} \quad 0 \quad \cdots \quad 0 \quad 0]$

in which $\overline{m}_{\mathrm{b}}$ denotes the mass per unit length of bridge, $\mathbf{N}_{\mathrm{b}j}$ (j =1, 2, …, $n_{\mathrm{b}i}$) is the shape function matrix for the *j*-th element of the *i*-th bridge of order $1 \times \overline{n}_{\mathrm{b}i}$, and $\overline{n}_{\mathrm{b}i}$ is the total number of degrees of freedom of the *i*-th multi-span continuous bridge. It should be noted for $\mathbf{N}_{\mathrm{b}j}$ that, apart from those elements corresponding to four DOFs of the two nodes of the *j*-th element, all other elements are zero.

The stiffness sub-matrix $\mathbf{K}_{\mathrm{bb}}$ of order $\overline{N}_{\mathrm{b}} \times \overline{N}_{\mathrm{b}}$ of bridges can be written as

$$\mathbf{K}_{\mathrm{bb}} = \mathrm{diag}[\mathbf{K}_{\mathrm{b1}} \quad \mathbf{K}_{\mathrm{b2}} \quad \cdots \quad \mathbf{K}_{\mathrm{b}N_{\mathrm{b}}}] \tag{13}$$

where $\mathbf{K}_{\mathrm{b}i}$ (i =1, 2, …, N_{b}) of order $\overline{n}_{\mathrm{b}i} \times \overline{n}_{\mathrm{b}i}$ denotes the stiffness matrix of the *i*-th multi-span continuous bridge. The stiffness matrix $\mathbf{K}_{\mathrm{b}i}$ can be written in terms of the overall stiffness matrix $\mathbf{K}_{\mathrm{b}i1}$ of the *i*-th bridge itself and the overall stiffness matrix $\mathbf{K}_{\mathrm{b}i2}$ induced by the stiffness of ballast on the *i*-th bridge as

$$\mathbf{K}_{\mathrm{b}i} = \mathbf{K}_{\mathrm{b}i1} + \mathbf{K}_{\mathrm{b}i2} \tag{14}$$

with $$\mathbf{K}_{\mathrm{b}i1}=\sum_{j=1}^{n_{\mathrm{b}i}}\int_{0}^{l_{\mathrm{b}}}E_{\mathrm{b}}I_{\mathrm{b}}\mathbf{N}_{\mathrm{b}j}''^{\mathrm{T}}\mathbf{N}_{\mathrm{b}j}''d\xi$$

$$\mathbf{K}_{\mathrm{b}i2}=\sum_{g=1}^{N_{\mathrm{sb}i}}k_{\mathrm{sb}}\mathbf{N}_{\mathrm{b},g}^{\mathrm{T}}\mathbf{N}_{\mathrm{b},g}$$

$$\mathbf{N}_{\mathrm{b},g}=[0\quad 0\quad\cdots\quad 0\quad N_{\mathrm{b},1}\quad N_{\mathrm{b},2}\quad N_{\mathrm{b},3}\quad N_{\mathrm{b},4}\quad 0\quad\cdots\quad 0\quad 0]_{\xi=\xi_{\mathrm{b},g}}$$

where E_{b} denotes Young's modulus of the bridge, I_{b} is the constant moment of inertia of the bridge cross-section, $N_{\mathrm{sb}i}$ denotes the total number of discrete ballast segments on the *i*-th bridge, $\mathbf{N}_{\mathrm{b},g}$ (*g*=1, 2, …, $N_{\mathrm{sb}i}$) of order $1\times\overline{n}_{\mathrm{b}i}$ is the shape function matrix of the bridge element evaluated at the position of the *g*-th discrete ballast segment, and $\xi_{\mathrm{b},g}$ denotes the distance between the *g*-th discrete ballast segment and the left node of the bridge element supporting it, as shown in Fig. 5. It should be noted for $\mathbf{N}_{\mathrm{b},g}$ (*g*=1, 2, …, $N_{\mathrm{sb}i}$) that, apart from those elements corresponding to four DOFs of the two nodes of the bridge element containing the *g*-th discrete ballast, all other elements are zero.

Similarly, the damping sub-matrix $\mathbf{C}_{\mathrm{bb}}$ of order $\overline{N}_{\mathrm{b}}\times\overline{N}_{\mathrm{b}}$ of bridges can be written as

$$\mathbf{C}_{\mathrm{bb}}=\mathrm{diag}[\mathbf{C}_{\mathrm{b}1}\quad\mathbf{C}_{\mathrm{b}2}\quad\cdots\quad\mathbf{C}_{\mathrm{b}N_{\mathrm{b}}}] \tag{15}$$

where $\mathbf{C}_{\mathrm{b}i}$ (i =1, 2, …, N_{b}) of order $\overline{n}_{\mathrm{b}i}\times\overline{n}_{\mathrm{b}i}$ denotes the damping matrix of the *i*-th multi-span continuous bridge. The damping matrix $\mathbf{C}_{\mathrm{b}i}$ can be written in terms of the overall damping matrix $\mathbf{C}_{\mathrm{b}i1}$ of the *i*-th bridge itself and the overall damping matrix $\mathbf{C}_{\mathrm{b}i2}$ induced by the damping of ballast on the *i*-th bridge as

$$\mathbf{C}_{\mathrm{b}i}=\mathbf{C}_{\mathrm{b}i1}+\mathbf{C}_{\mathrm{b}i2} \tag{16}$$

with $$\mathbf{C}_{\mathrm{b}i2}=\sum_{g=1}^{N_{\mathrm{sb}i}}c_{\mathrm{sb}}\mathbf{N}_{\mathrm{b},g}^{\mathrm{T}}\mathbf{N}_{\mathrm{b},g}$$

Based on the assumption of Rayleigh damping, the damping matrix $\mathbf{C}_{\mathrm{b}i1}$ of order $\overline{n}_{\mathrm{b}i}\times\overline{n}_{\mathrm{b}i}$ of the *i*-th bridge itself can be computed as

$$\mathbf{C}_{\mathrm{b}i1}=\alpha\cdot\mathbf{M}_{\mathrm{b}i}+\beta\cdot\mathbf{K}_{\mathrm{b}i1} \tag{17}$$

Given the damping ratio ζ and the first two natural circular frequencies of vibration of the bridge ω_1 and ω_2, the coefficients can be determined as $\alpha = 2\zeta\omega_1\omega_2/(\omega_1+\omega_2)$ and $\beta = 2\zeta/(\omega_1+\omega_2)$ [4].

3. 6 Sub-matrices for vehicle-rail interaction

The sub-matrices for vehicle-rail interaction are marked with subscript "vr" or "rv". The sub-matrices $\mathbf{K}_{\mathrm{vr}}$, $\mathbf{K}_{\mathrm{rv}}$, $\mathbf{C}_{\mathrm{vr}}$ and $\mathbf{C}_{\mathrm{rv}}$ can be worked out similarly. Their full expressions are not given here and can be found in reference [9].

3. 7 Sub-matrices for rail-sleeper interaction

The sub-matrices for rail-sleeper interaction are marked with subscript "rs" or "sr". The stiffness sub-matrix $\mathbf{K}_{\mathrm{rs}}$ and the damping sub-matrix $\mathbf{C}_{\mathrm{rs}}$ of order $N_{\mathrm{r}} \times N_{\mathrm{s}}$ for the stiffness and damping, respectively, of pads between the rail and sleepers can be written as

$$\mathbf{K}_{\mathrm{rs}} = \begin{bmatrix} -k_{\mathrm{rs}}\mathbf{N}_{\mathrm{r},1}^{\mathrm{T}} & -k_{\mathrm{rs}}\mathbf{N}_{\mathrm{r},2}^{\mathrm{T}} & \cdots & -k_{\mathrm{rs}}\mathbf{N}_{\mathrm{r},u}^{\mathrm{T}} & \cdots & -k_{\mathrm{rs}}\mathbf{N}_{\mathrm{r},N_{\mathrm{s}}}^{\mathrm{T}} \end{bmatrix} \tag{18}$$

$$\mathbf{C}_{\mathrm{rs}} = \begin{bmatrix} -c_{\mathrm{rs}}\mathbf{N}_{\mathrm{r},1}^{\mathrm{T}} & -c_{\mathrm{rs}}\mathbf{N}_{\mathrm{r},2}^{\mathrm{T}} & \cdots & -c_{\mathrm{rs}}\mathbf{N}_{\mathrm{r},u}^{\mathrm{T}} & \cdots & -c_{\mathrm{rs}}\mathbf{N}_{\mathrm{r},N_{\mathrm{s}}}^{\mathrm{T}} \end{bmatrix} \tag{19}$$

In addition, one also has $\mathbf{K}_{\mathrm{sr}} = \mathbf{K}_{\mathrm{rs}}^{\mathrm{T}}$ and $\mathbf{C}_{\mathrm{sr}} = \mathbf{C}_{\mathrm{rs}}^{\mathrm{T}}$.

3. 8 Sub-matrices for sleeper-bridge interaction

The sub-matrices for sleeper-bridge interaction are marked with subscript "sb" or "bs". The stiffness sub-matrix $\mathbf{K}_{\mathrm{bs}}$ of order $\overline{N}_{\mathrm{b}} \times N_{\mathrm{s,b}}$ induced by the stiffness of ballast between the bridge and sleepers can be written as

$$\mathbf{K}_{\mathrm{bs}} = \mathrm{diag}[\mathbf{K}_{\mathrm{bs}1} \quad \mathbf{K}_{\mathrm{bs}2} \quad \cdots \quad \mathbf{K}_{\mathrm{bs}N_{\mathrm{b}}}] \tag{20}$$

where $\mathbf{K}_{\mathrm{bs}i}$ (i =1, 2, …, N_{b}) of order $\overline{n}_{\mathrm{b}i} \times \overline{n}_{\mathrm{s,b}i}$ denotes the stiffness matrix induced by the stiffness of ballast between the i-th bridge and sleepers on it, $N_{\mathrm{s,b}}$ denotes the total number of sleepers on bridges, and $\overline{n}_{\mathrm{s,b}i}$ denotes the number of sleepers on the i-th bridge. The stiffness matrix $\mathbf{K}_{\mathrm{bs}i}$ can be written as

$$\mathbf{K}_{\mathrm{bs}i} = \begin{bmatrix} -k_{\mathrm{sb}}\mathbf{N}_{\mathrm{b},1}^{\mathrm{T}} & -k_{\mathrm{sb}}\mathbf{N}_{\mathrm{b},2}^{\mathrm{T}} & \cdots & -k_{\mathrm{sb}}\mathbf{N}_{\mathrm{b},g}^{\mathrm{T}} & \cdots & -k_{\mathrm{sb}}\mathbf{N}_{\mathrm{b},\overline{n}_{\mathrm{s,b}i}}^{\mathrm{T}} \end{bmatrix} \tag{21}$$

Similarly, the damping sub-matrix $\mathbf{C}_{\mathrm{bs}}$ of order $\overline{N}_{\mathrm{b}} \times N_{\mathrm{s,b}}$ induced by the damping of ballast between the bridge and sleepers on it can be written as

$$\mathbf{C}_{\mathrm{bs}} = \mathrm{diag}[\mathbf{C}_{\mathrm{bs1}} \quad \mathbf{C}_{\mathrm{bs2}} \quad \cdots \quad \mathbf{C}_{\mathrm{bs}N_{\mathrm{b}}}] \tag{22}$$

with $$\mathbf{C}_{\mathrm{bs}i} = \left[-c_{\mathrm{sb}}\mathbf{N}_{\mathrm{b},1}^{\mathrm{T}} \quad -c_{\mathrm{sb}}\mathbf{N}_{\mathrm{b},2}^{\mathrm{T}} \quad \cdots \quad -c_{\mathrm{sb}}\mathbf{N}_{\mathrm{b},g}^{\mathrm{T}} \quad \cdots \quad -c_{\mathrm{sb}}\mathbf{N}_{\mathrm{b},\overline{n}_{\mathrm{s},bi}}^{\mathrm{T}} \right]$$

In addition, one also has $\mathbf{K}_{\mathrm{sb}} = \mathbf{K}_{\mathrm{bs}}^{\mathrm{T}}$ and $\mathbf{C}_{\mathrm{sb}} = \mathbf{C}_{\mathrm{bs}}^{\mathrm{T}}$.

3. 9 Force sub-vectors of vehicles, rail, sleepers and bridge

The force sub-vectors $\mathbf{F}_{\mathrm{v}}$ of order $6N_{\mathrm{v}} \times 1$ of vehicles and $\mathbf{F}_{\mathrm{r}}$ of order $N_{\mathrm{r}} \times 1$ of rail can be worked out accordingly. Their full expressions are not given here and can be found in reference [9]. Each element in the force sub-vectors $\mathbf{F}_{\mathrm{s}}$ of order $N_{\mathrm{s}} \times 1$ of sleepers and $\mathbf{F}_{\mathrm{b}}$ of order $\overline{N}_{\mathrm{b}} \times 1$ of bridges is zero.

Eq. (3) can be solved by the step-by-step integration method, such as Newmark-β method [17] or Wilson-θ method [18], to obtain simultaneously the dynamic responses of train, track and bridges. Eq. (3) has been written on the assumption that N_{v} vehicles are acting on the track concerned. If certain vehicles are not on the track concerned, the corresponding rows and columns of the matrix equation should be deleted.

4 Numerical examples

The present element is applied in the following three examples. The first one is to illustrate the efficiency of the present element. The second one is to investigate the effect of LRE on the dynamic responses of the train-track-bridge interaction system. The last one is to investigate the effects of two types of track models on the dynamic responses of vehicle, rail, and bridge. Five identical vehicles are considered to run over a track-bridge coupling system shown in Fig. 4. The parameters of vehicle are listed in Table 1. In the track-bridge coupling system, the central part of railway track is supported on bridge, while the left and right parts of railway track are supported on embankment. The railway track is assumed to be smooth and

continuous throughout, while the lengths of left and right parts of track considered are both 20 m. The parameters of bridge and track listed respectively in Tables 1 and 2 are adopted in this section unless otherwise stated. Two types of bridge models are applied in the sections 4.1 and 4.2. One comprises three single-span simply supported bridges each of 20 m, with a total length of 60 m. The other is a 3-span continuous bridge with spans of 20 m. To solve the equation of motion for the train-track-bridge interaction system, the Wilson-θ method is used with $\theta = 1.4$ and moving length of 0.1 m of vehicles along track for each time step. The analysis is performed by applying the speed from 10 m/s to 200 m/s at 2.5 m/s interval.

4.1 Example 1: Two types of rail-bridge coupling elements of equal LRE and unequal LBE

To illustrate the efficiency of the present element, the following two cases are studied.

Case I: Analysis using rail-bridge coupling element of equal length, with LRE = LBE = 0.625 m; and

Case II: Analysis using the present element, with LRE = 0.625 m and LBE = 5.0 m.

It should be noted that LRE is the same for Cases I and II, but LBE is unequal. The dynamic responses of vehicle, rail, sleeper and bridge of two bridge configurations for Cases I and II at various vehicle speeds are plotted in Figs. 6-12. For convenience hereafter, SB denotes the arrangement of 3 simply supported bridges while CB denotes a 3-span continuous bridge. Fig. 6 shows the maximum vertical acceleration at the centroid of the last car body. Figs. 7 and 8 show respectively the maximum vertical displacement and maximum bending moment of the rail at the middle of central span. Figs. 9 and 10 show respectively the maximum vertical displacement and maximum vertical acceleration of the sleeper immediately to the right of the middle of central span. Figs. 11 and 12, respectively, plot the maximum vertical displacement and maximum bending moment of the bridge at the middle of central span. The simply supported bridges, being less stiff, display resonance roughly at a train speed of 160 m/s and mostly give higher dynamic responses compared with those of the continuous bridge. For the same bridge model, excellent agreement between the dynamic responses of

Cases I and II can be observed from Figs. 6-12 as elaborated below. The major difference here is that Case I uses 8 bridge elements to model a bridge length of LBE = 5.0 m, while Case II uses just one bridge element. In spite of the theoretical discrepancies between the displacement functions of Cases I and II, excellent agreement is obtained because the structural response is largely governed by the much higher flexural rigidity of bridge.

Compared with the rail-bridge coupling element of equal length, the present element helps to save computer time because of the drastic reduction of DOFs. For example, the total CPU times for Cases I and II for 3 simply supported bridges are 18972 s and 10413 s on a 2.4 GHz personal computer, respectively, and the ratio of the latter to the former is 0.549. Similarly, the total CPU times for Cases I and II for a continuous bridge are 18455 s and 10155 s, respectively, and the ratio of the latter to the former is 0.55.

4.2 Example 2: Two types of rail-bridge coupling elements of unequal LRE and equal LBE

To investigate the effect of LRE on the dynamic responses of the train-track-bridge interaction system, the following two cases are studied.

Case II: Analysis using the present element, with LRE = 0.625 m and LBE = 5.0 m; and

Case III: Analysis using rail-bridge coupling element of equal length, with LRE = LBE = 5.0 m.

It can be seen that LRE is unequal for Cases II and III, but LBE is the same. The dynamic responses of vehicle, rail, sleeper and bridge of two bridge configurations for Cases II and III at various vehicle speeds are plotted in Figs. 13-19. Fig. 13 shows the maximum vertical acceleration at the centroid of the last car body. Figs. 14 and 15 show respectively the maximum vertical displacement and maximum bending moment of the rail at the middle of central span. Figs. 16 and 17 show respectively the maximum vertical displacement and maximum vertical acceleration of the sleeper immediately to the right of the middle of central span. Figs. 18 and 19, respectively, plot the maximum vertical displacement and maximum bending moment of the bridge at the middle of central span. Figs. 14 and 15 show that, for the same bridge configuration, there are obvious

differences between Cases II and III for the rail responses. Figure 16 shows negligible difference in maximum vertical displacement of sleeper between Cases II and III for the same bridge configuration. However, Figure 17 shows obvious difference in maximum vertical acceleration of sleeper between Cases II and III for the same bridge configuration, as acceleration is more sensitive to small variations than displacement. As seen from Figs. 18 and 19, the differences between Cases II and III for the bridge responses are insignificant. From Tables 1 and 2, the ratio of flexural rigidity of bridge to that of rail is about 8460, while the ratio of mass per unit length of bridge to that of rail is about 281. As the stiffness and mass of the bridge are much larger than those of the rail, the bridge responses are little affected by the modelling of the rail. However if accurate rail responses are needed, sufficiently fine mesh should be adopted for the rail. Therefore the rail responses given by Case II in Figs. 14 and 15 are more accurate than those of Case III. This is especially the case for bending moments.

4.3 Example 3: The effects of two types of track models on the dynamic responses of vehicle, rail, and bridge

In this example, let us consider a simply supported bridge of 20 m length with two types of track models. One is a one-layer track model with sleeper ignored, and the other one is a two-layer track model with sleeper considered applied in this paper. The total length of each track model is 60 m. LRE = 0.625 m and LBE = 5.0 m are adopted. The stiffness k_{rb} of discrete spring between rail and bridge in the one-layer track model can be obtained by considering k_{rs} and k_{sb} as series connection in the two-layer track model with sleeper ignored, i.e., $k_{\mathrm{rb}} = k_{\mathrm{rs}} \cdot k_{\mathrm{sb}} /(k_{\mathrm{rs}} + k_{\mathrm{sb}})$. Similarly, the damping coefficient c_{rb} of discrete damper between rail and bridge in the one-layer track model can be obtained by $c_{\mathrm{rb}} = c_{\mathrm{rs}} \cdot c_{\mathrm{sb}} /(c_{\mathrm{rs}} + c_{\mathrm{sb}})$. To study the effect the mass m_{s} of a sleeper in the two-layer track model on the dynamic responses of vehicle, rail, and bridge, three masses of 340 kg, 680 kg, and 1020 kg are applied, respectively. The other parameters are the same as

Tables 1 and 2.

To observe the effects of track model on the dynamic responses of vehicle, rail, and bridge, the deviation D_e between the dynamic response based on the one-layer track model and that based on the two-layer track model is determined according to the definition

$$D_e = \frac{dyn_1 - dyn_2}{dyn_2} \times 100\% \tag{23}$$

where dyn_1 and dyn_2 are the dynamic responses based on the one-layer and two-layer track models, respectively. The deviations of the dynamic responses of vehicle, rail, and bridge at various vehicle speed based on the one-layer track model and the two-layer track model with m_s = 340 kg, 680 kg, and 1020 kg are plotted in Figs. 20-24. Fig. 20 shows the deviations of maximum vertical acceleration at the centroid of the last car body. Figs. 21 and 22 show respectively the deviations of the maximum vertical displacement and maximum bending moment of the rail at the mid-span of the bridge. Figs. 23 and 24 plot the deviations of the maximum vertical displacement and maximum bending moment of the bridge at the mid-span, respectively. It can be seen, from Figs. 20-24, that there are deviations of the dynamic responses based on the one-layer and two-layer track models, and the maximum deviations of the dynamic responses increase with the increase of the mass of sleeper. The reason for which will be explained as follows.

From Yang et al. [19], it is known that the dimensionless resonant speed parameter is

$$S_{res} = d/(2nL_b) \tag{24}$$

where d is the vehicle length, L_b the bridge span length, and n is positive integer. Furthermore, from Yang et al. [20], the speed parameter S is taken as

$$S = v\pi/(\omega_1 L_b) \tag{25}$$

where ω_1 is the natural fundamental circular frequency of bridge, v is the seed of vehicle. Substituting Eq. (25) into Eq. (24), the resonant speed can be written as

$$v = \omega_1 d /(2\pi \cdot n) \tag{26}$$

From Frýba [21], the natural fundamental circular frequency of a simply supported bridge is

$$\omega_1 = \pi^2 \cdot \sqrt{E_b I_b /(\overline{m}_b \cdot L_b^4)} \tag{27}$$

For the bridge taking into account the effect of track, the $\overline{m}_b$ in Eq. (27) should be included the mass of track. Therefore, for the two-layer track model, when the mass m_s of sleeper increases, the $\overline{m}_b$ in Eq. (27) will increase and the ω_1 in Eq. (27) will decrease. Furthermore, the resonant speed v in Eq. (26) will also decrease. This can be verified by Figs. 25 and 26. Figs. 25 and 26 plot the maximum vertical displacements and maximum bending moments of the bridge at the mid-span with the one-layer track model and the two-layer track model of m_s = 340 kg, 680 kg, and 1020 kg, respectively. It can be seen from Figs. 25 and 26 that , with the increase of the mass of sleeper, the resonant speed decreases and the shift distance of the curve increases, which results in that the difference between the curve based on the two-layer track model and that based on the one-layer track model at a certain speed increases.

5 Concluding remarks

Based on the obvious difference of flexural rigidity between rail and bridge, the rail-bridge coupling element of unequal lengths has been presented. The dynamic responses of a train-track-bridge interaction system with two types of bridge configurations have been modelled using rail-bridge coupling elements of unequal lengths and equal lengths. In addition, the effects of two types of track models on the dynamic responses of vehicle, rail, and bridge have been investigated. From the numerical results, the following conclusions can be reached.

(1) In modelling a train-track-bridge interaction system, the dynamic responses obtained by the present rail-bridge coupling element of unequal lengths agree very well with those obtained by the rail-bridge coupling element of equal length if rail elements of the same length are used. In addition, the present element helps to

save computer time.

(2) In analysis of a train-track-bridge interaction system using rail-bridge coupling elements having the same length of bridge element, the influence of length of rail element on the rail responses is significant, but the influence of length of rail element on the bridge responses is insignificant.

(3) If one is interested in the dynamic responses of the entire train-track-bridge interaction system, the present element with shorter rail elements and a longer bridge element may be adopted. This not only gives satisfactory results, but also helps to save computer time.

(4) The one-layer track model with sleeper ignored and the two-layer track model with sleeper considered affect the natural frequency of bridge. Therefore, there are deviations of the dynamic responses of vehicle, rail, and bridge based on the one-layer and two-layer track models, and the maximum deviations increase with the increase of the mass of sleeper.

(5) The approach of the present coupling element can be extended to composite structures with obvious difference in flexural rigidity.

Acknowledgements

The authors thank Prof. M. Cross, Editor-in-Chief, Applied Mathematical Modelling, and the anonymous reviewer for their valuable and helpful comments. The work was supported by the National Natural Science Foundation of China (grants 51078360 and 50938008), and Hunan Provincial Natural Science Foundation of China (grant 10JJ3059).

References

[1] R. Le, B. Ripke, M. Zacher, Ballast mats on high speed bridges. In: Proceedings of The Fourth European Conference on Structural Dynamics, EURODYN'99, Prague (Czech Republic), 7-10 June 1999, pp.

699-703.

[2] Y. S. Cheng, F. T. K. Au, Y. K. Cheung, Vibration of railway bridges under a moving train by using bridge-track-vehicle element, Eng. Struct. 23(2001) 1597-1606.

[3] M. Majka, M. Hartnett, C. Bowe, D. O'Dwyer, Dynamic train-track-bridge interaction on example of the boyne viaduct, ICCST '02 Proceedings of the Sixth Conference on Computational Structures Technology, Civil-Comp Press Edinburgh, UK, 2002, 339-340.

[4] Y. S. Wu, Y. B. Yang, Steady-state response and riding comfort of trains moving over a series of simply supported bridges, Eng. Struct. 25(2003) 251-265.

[5] Q. Y. Zeng, X.R. Guo, Theory and Application of Vibration Analysis of Train-Bridge Time-Dependent System, China Railway Publishing House, Beijing, 1999 (in Chinese).

[6] Q. Y. Zeng, The principle of a stationary value of total potential energy of dynamic system, J. Huazhong Univ. Sci. Technol. 28(1)(2000) 1–3 (in Chinese).

[7] P. Lou, A vehicle-track-bridge interaction element considering vehicle's pitching effect, Finite Elem. Anal. Des. 41(2005) 397-427.

[8] P. Lou, Q. Y. Zeng, Formulation of equations of motion of finite element form for vehicle-track-bridge interaction system with two types of vehicle models, Int. J. Numer. Meth. Eng. 62(2005) 435-474.

[9] P. Lou, Finite element analysis for train-track-bridge interaction system, Arch. Appl. Mech. 77(2007) 707-728.

[10] W. M. Zhai, C. B. Cai, K. Y. Wang, Mechanism and model of high-speed train-track-bridge dynamic interaction, China Civ. Eng. J. 38(11)(2005) 132–137 (in Chinese).

[11] Y. S. Lee, S. H. Kim, J. Jung, Three-dimensional finite element analysis model of high-speed train-track-bridge dynamic interactions, Adv. in Struct. Eng. 8(2005) 513-528.

[12] B. Biondi, G. Muscolino, A. Sofi, A substructure approach for the dynamic analysis of train-track-bridge

system, Comput. and Struct. 83(2005) 2271-2281.

[13] X. Li, D. Liu, Z . Jin, Analysis of train-track-bridge coupled vibration of a railway long-span suspension bridge, Steel Constr. 25(12)(2010) 6–12,71 (in Chinese).

[14] Y. S. Wu, Y. B. Yang, J. D. Yau, Three-Dimensional analysis of train-rail-bridge interaction problems, Vehicle Syst. Dyn. 36(2001) 1-35.

[15] Z. M. Zhai, Vehicle-Track Coupling Dynamics (Third Edition), China Science Publishing House, Beijing, 2007 (in Chinese).

[16] J. Y. Pan, M. M. Gao, Dynamic Analysis of Vehicle-Track-Bridge System, China Railway Publishing House, Beijing, 2008 (in Chinese).

[17] N. M. Newmark, A method of computation for structural dynamics, J. Eng. Mech. Div. Proc. Am. Soc. Civil Engrs. 85(1959) 67-94.

[18] K. J. Bathe, E. L. Wilson, Numerical Methods in Finite Element Analysis, Prentice-Hall Inc., Englewood Cliffs, N.J., 1976.

[19] Y. B. Yang, J. D. Yau, L. C. Hsu, Vibration of simple beams due to trains moving at high speeds, Eng. Struct. 19(1997) 936-944.

[20] Y. B. Yang, C. H. Chang, J. D. Yau, An element for analyzing vehicle-bridge systems considering vehicle's pitching effect, Int. J. Numer. Meth. Eng. 46(1999) 1031-1047.

[21] L . Frýba , Dynamics of Railway Bridges. Thomas Telford, London, 1996.

Figures:

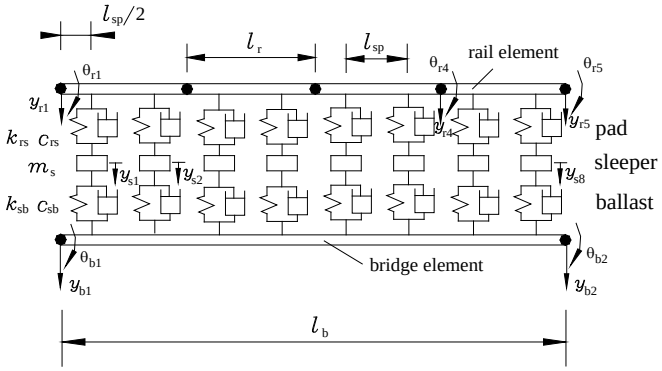

Figure 1. A typical rail-bridge coupling element of unequal lengths

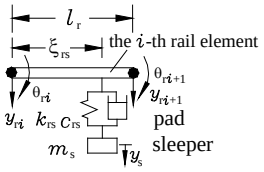

Figure 2. A sleeper and pad attached to the *i*-th rail element

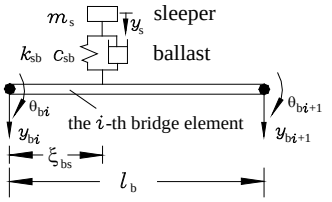

Figure 3. A sleeper and ballast attached to the *i*-th bridge element

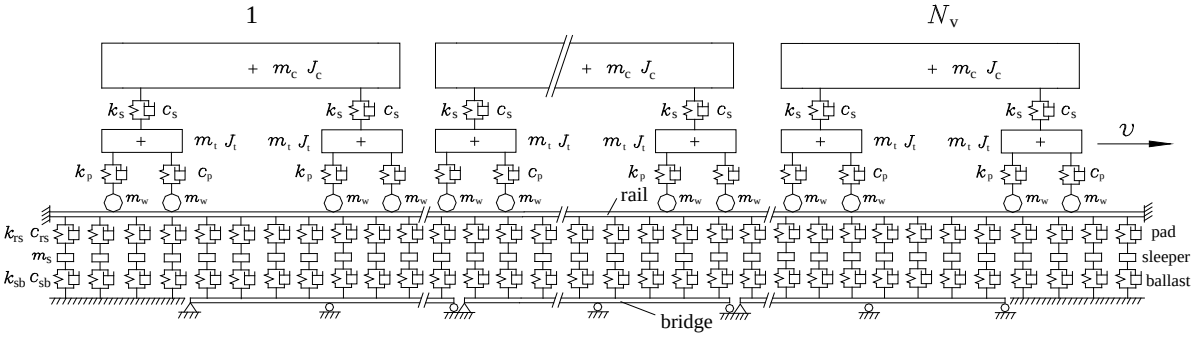

Figure 4. A typical train-track-bridge interaction system

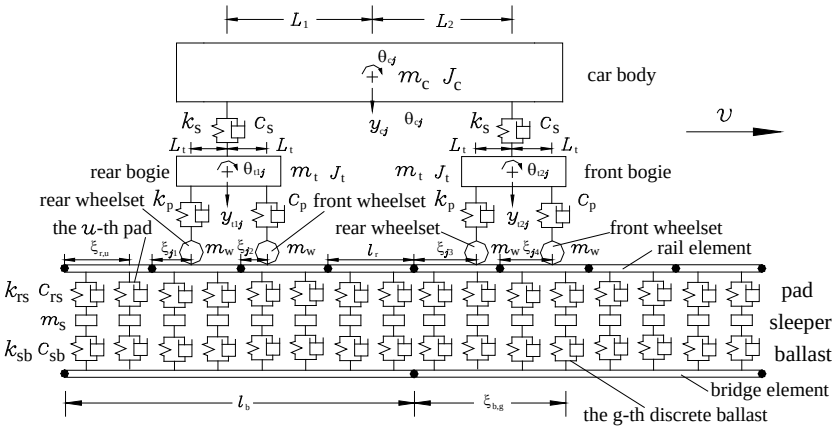

Figure 5. The *j*-th vehicle running on rail-bridge coupling elements of unequal lengths

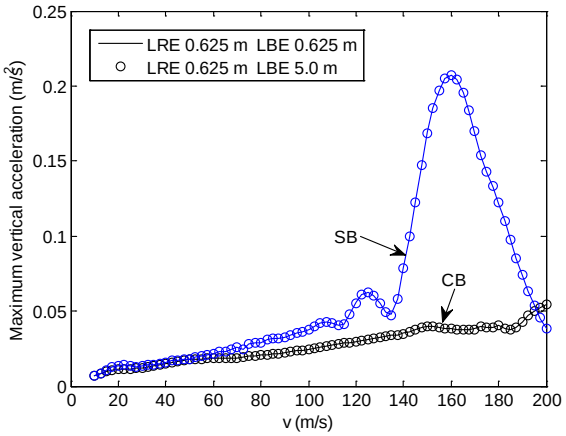

Figure 6. The maximum vertical acceleration at centroid of last car body at various speeds for Cases I and II (SB: simply supported bridge; CB: continuous bridge)

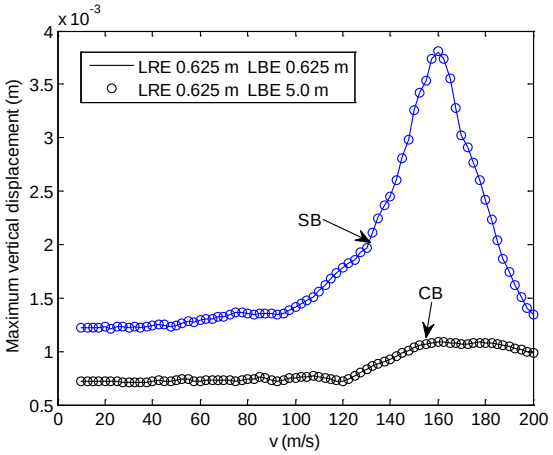

Figure 7. The maximum vertical displacement of rail at middle of central span at various train speeds for Cases I and II (SB: simply supported bridge; CB: continuous bridge)

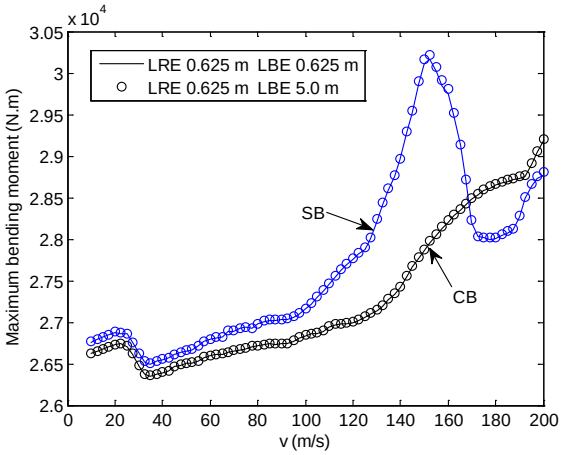

Figure 8. The maximum bending moment of rail at middle of central span at various train speeds for Cases I and II (SB: simply supported bridge; CB: continuous bridge)

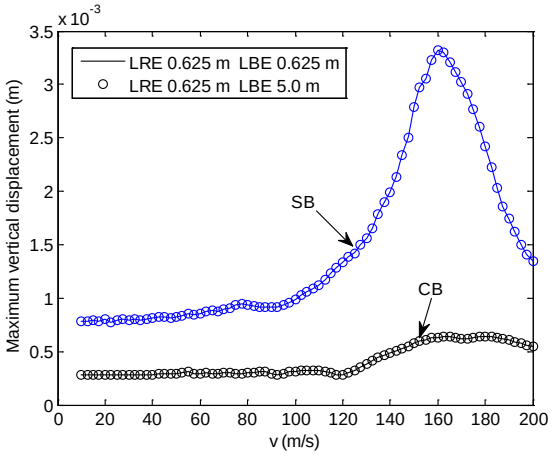

Figure 9. The maximum vertical displacement of the sleeper immediately to the right of middle of central span at various train speeds for Cases I and II (SB: simply supported bridge; CB: continuous bridge)

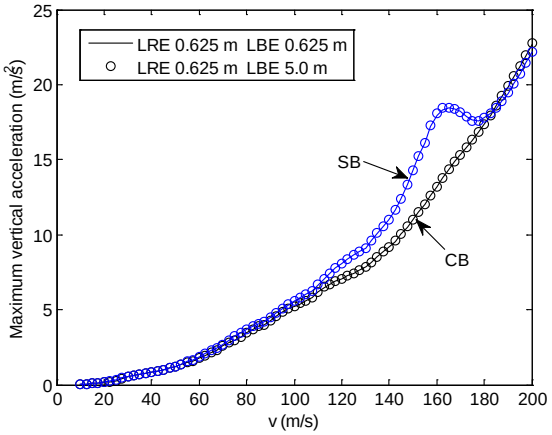

Figure 10. The maximum vertical acceleration of the sleeper immediately to the right of middle of central span at various train speeds for Cases I and II (SB: simply supported bridge; CB: continuous bridge)

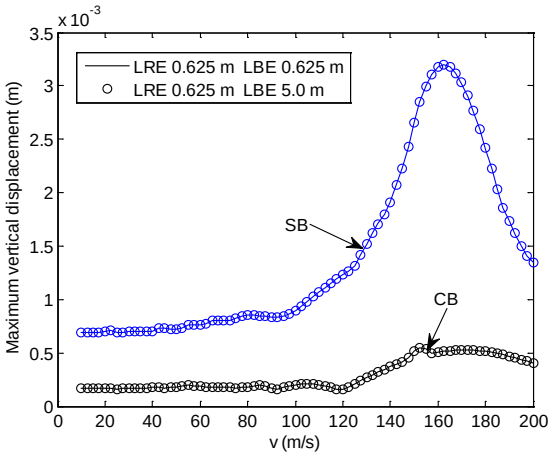

Figure 11. The maximum vertical displacement of bridge at middle of central span at various train speeds for Cases I and II (SB: simply supported bridge; CB: continuous bridge)

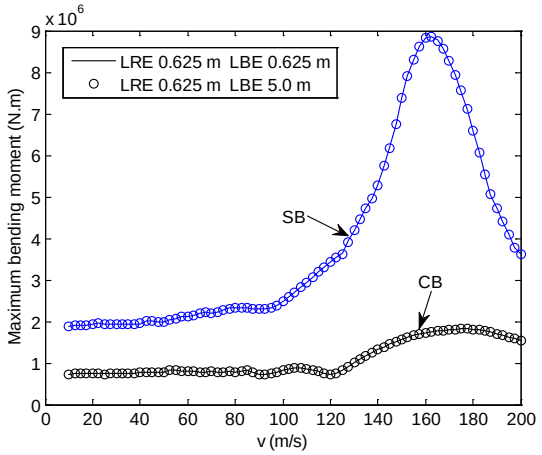

Figure 12. The maximum bending moment of bridge at middle of central span at various train speeds for Cases I and II (SB: simply supported bridge; CB: continuous bridge)

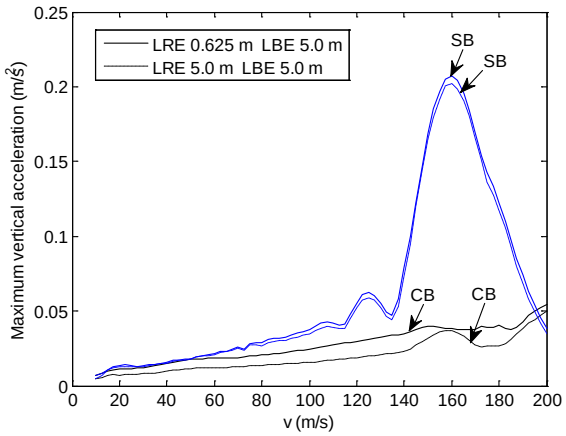

Figure 13. The maximum vertical acceleration at centroid of last car body at various train speeds for Cases II and III (SB: simply supported bridge; CB: continuous bridge)

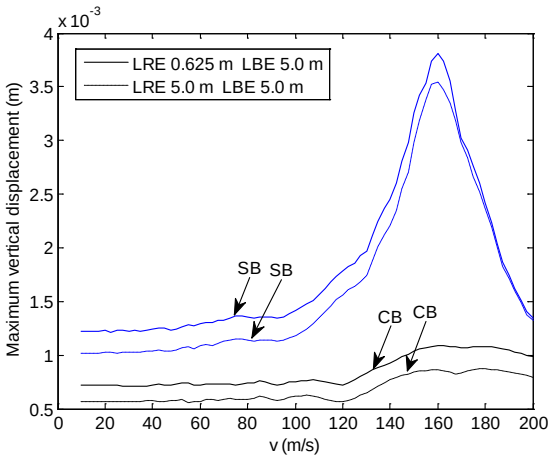

Figure 14. The maximum vertical displacement of rail at middle of central span at various train speeds for Cases II and III (SB: simply supported bridge; CB: continuous bridge)

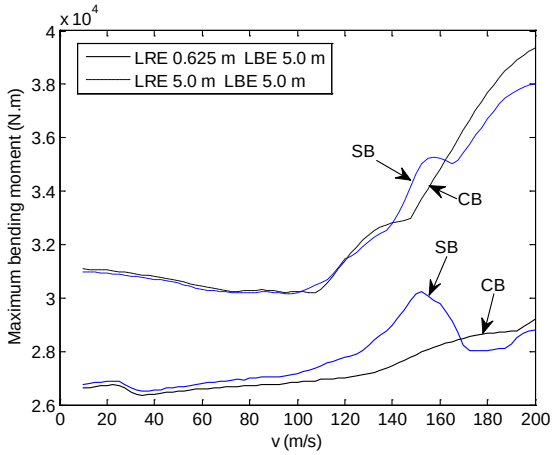

Figure 15. The maximum bending moment of rail at middle of central span at various train speeds for Cases II and III (SB: simply supported bridge; CB: continuous bridge)

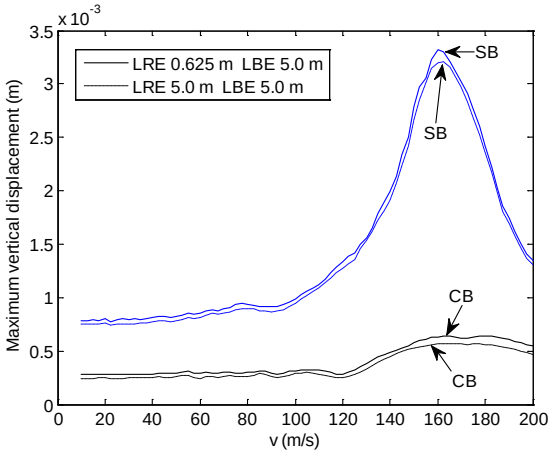

Figure 16. The maximum vertical displacement of the sleeper immediately to the right of middle of central span at various train speeds for Cases II and III (SB: simply supported bridge; CB: continuous bridge)

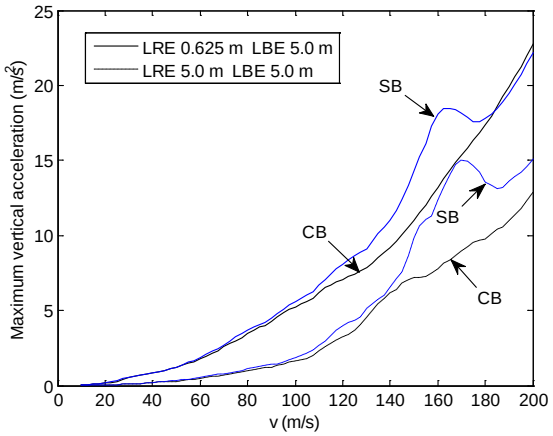

Figure 17. The maximum vertical acceleration of the sleeper immediately to the right of middle of central span at various train speeds for Cases II and III (SB: simply supported bridge; CB: continuous bridge)

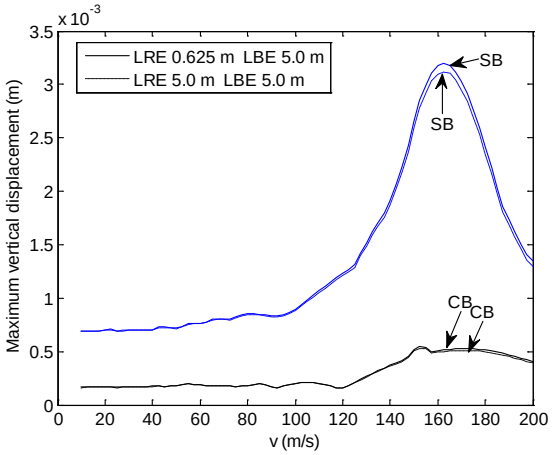

Figure 18. The maximum vertical displacement of bridge at middle of central span at various train speeds for Cases II and III (SB: simply supported bridge; CB: continuous bridge)

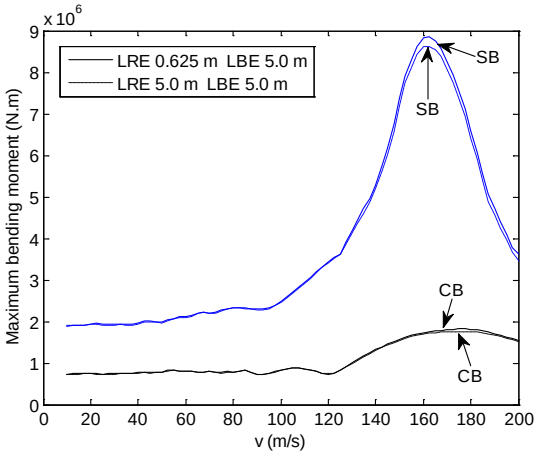

Figure 19. The maximum bending moment of bridge at middle of central span at various train speeds for Cases II and III (SB: simply supported bridge; CB: continuous bridge)

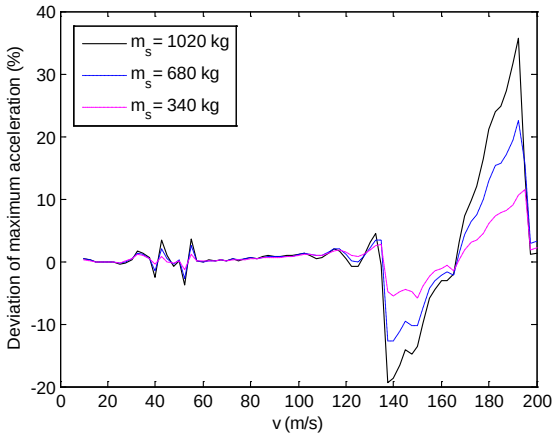

Figure 20. The deviations of maximum vertical acceleration at the centroid of the last car body at various speeds

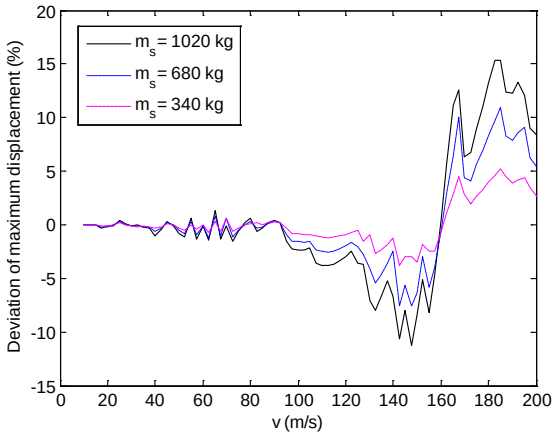

Figure 21. The deviations of the maximum vertical displacement of rail at the mid-span of the bridge at various speeds

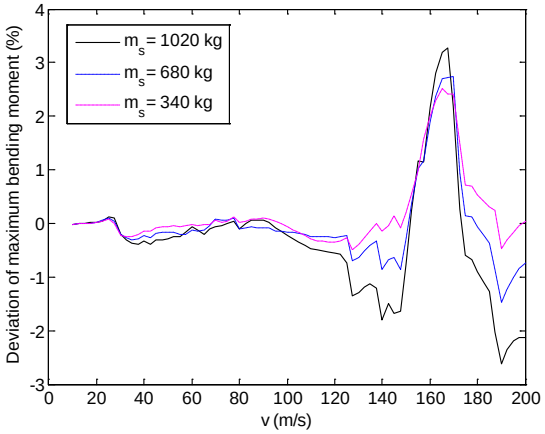

Figure 22. The deviations of the maximum benidng moment of rail at the mid-span of the bridge at various speeds

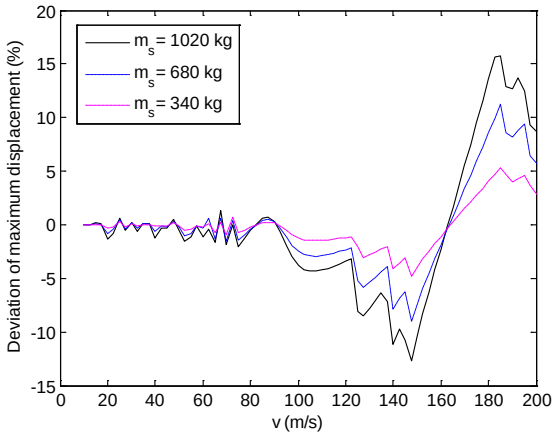

Figure 23. The deviations of the maximum vertical displacement of bridge at the mid-span at various speeds

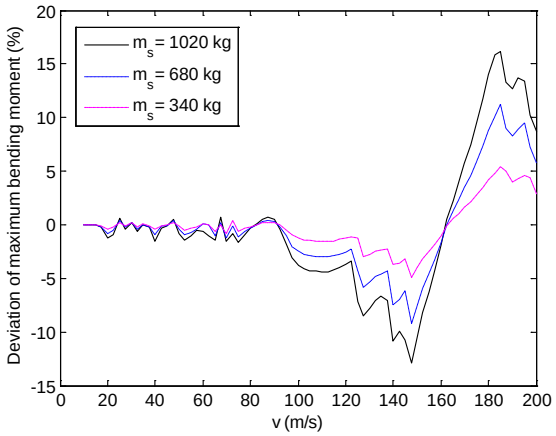

Figure 24. The deviations of the maximum bending moment of bridge at the mid-span at various speeds

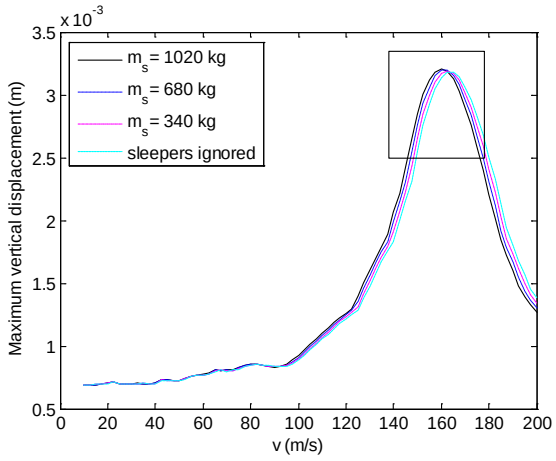

(a) full figure

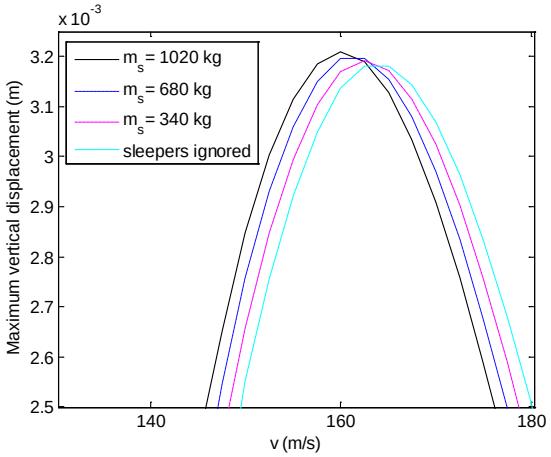

(b) local figure

Figure 25. The maximum vertical displacements of bridge at the mid-span with two types of track models at various speeds

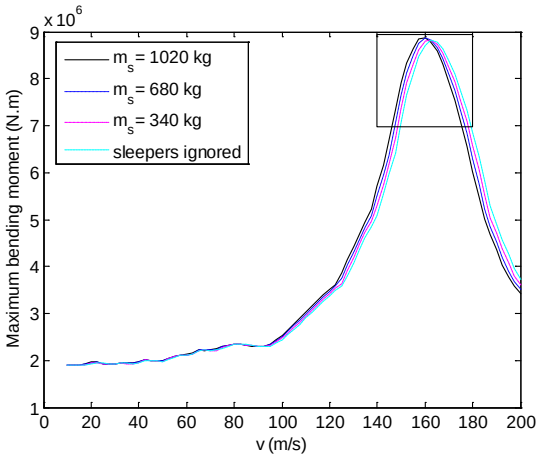

(a) full figure

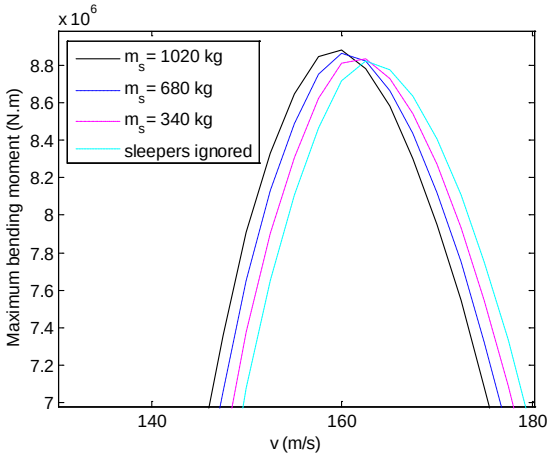

(b) local figure

Figure 26. The maximum bending moments of bridge at the mid-span with two types of track models at various speeds

Tables

Table 1. Parameters of vehicle and bridge in numerical examples

Notation	Parameter	Value
Vehicle		
m_c	Mass of car body	4.175×10^4 kg
J_c	Mass moment of inertia of car body	2.08×10^6 kg·m^2
L_d	Longitudinal distance between the centre of rear bogie of a 4-wheelset vehicle and the centre of front bogie of the following 4-wheelset vehicle	6.0 m
k_s	Spring stiffness of the second suspension system	5.3×10^5 N/m
c_s	Damping coefficient of the second suspension system	9.02×10^4 N·s/m
L_1	Longitudinal distance between the centres of gravity of car body and rear bogie	8.75 m
L_2	Longitudinal distance between the centres of gravity of car body and front bogie	8.75 m
m_t	Mass of a bogie frame	3.04×10^3 kg
J_t	Mass moment of inertia of a bogie frame	3.93×10^3 kg·m^2
L_t	Half of bogie axle base	1.25 m
k_p	Spring stiffness of the primary suspension system	1.18×10^6 N/m
c_p	Damping coefficient of the primary suspension system	3.92×10^4 N·s/m
m_w	Mass of a wheelset	1.78×10^3 kg
Bridge		
E_b	Young's modulus	2.943×10^{10} Pa
I_b	Moment of inertia	3.81 m^4
$\overline{m}_b$	Mass per unit length	3.4088×10^4 kg/m
ζ_b	Damping ratio	0.02

Table 2. Parameters of track

Notation	Parameter	Value
L_r	Total length of track structure concerned	100 m
E_r	Young's modulus	2.06×10^{11} Pa
I_r	Moment of inertia	$2\times3.217\times10^{-5}$ m^4
$\overline{m}_r$	Mass per unit length	2×60.64 kg/m
m_s	Mass of a sleeper	340 kg
l_{sp}	Spaces between two adjacent sleepers	0.625 m
k_{rs}	Stiffness of discrete spring reflecting the property of rail pad	$2\times6.0\times10^7$ N/m
c_{rs}	Damping coefficient of discrete damper reflecting the property of rail pad	$2\times7.5\times10^4$ N·s/m
k_{sb}	Stiffness of discrete spring reflecting the property of ballast	$2\times2.25\times10^8$ N/m
c_{sb}	Damping coefficient of discrete damper reflecting the property of ballast	$2\times6.0\times10^4$ N·s/m